INTERNATIONAL JOURNAL FOR NUMERICAL METHODS IN FLUIDS, VOL. 7, 793–823 (1987)

STUDIES IN NUMERICAL COMPUTATIONS OF RECIRCULATING FLOWS

I. P. CASTRO AND J. M. JONES*

Department of Mechanical Engineering, University of Surrey, Guildford Surrey, U.K.

SUMMARY

This paper considers the use of various finite differencing schemes for the computation of flows involving regions of recirculation. Standard first-order hybrid schemes, vector (or skew) schemes and second-order schemes are used to predict laminar flows in a channel containing a constriction and over a normal flat plate with a downstream splitter plate. In the former case the results are compared with those of other workers and with the implications of analytic theories for the viscous dominated flow around the sharp corner.

Attention is concentrated on the effects of errors arising from the use of non-uniform grids and it is shown that higher-order differencing schemes are generally much less susceptible to these than the simpler schemes. The major conclusion is that for flows containing regions where pressure gradients largely balance the convective terms in the momentum equations, in addition to other regions where convection and diffusion balance, higher order differencing schemes are likely to be essential if accurate predictions are required on grids without excessive numbers of nodes. It is argued that similar conclusions must hold for high Reynolds number turbulent flows.

KEY WORDS Finite Differencing Viscous Flow Flow with Recirculation

1. INTRODUCTION

Numerical predictions of complex turbulent flows, even those involving significant regions of separation, are becoming commonplace. However, it is generally agreed that in addition to the uncertainties concerning the turbulence modelling required, the numerical problems associated with such flows are usually much more serious than those encountered in solving, say, boundary-layer type flows. The most recent extensive exercise in comparing numerical predictions with experiments was the two-part AFOSR-HTTM Stanford Conference on Complex Turbulent Flows, fully reported by Kline *et al.*[1] It is significant that despite the industrial importance of separated flows, only three data sets were considered adequate for comparison with numerical predictions (compared with 63 for attached flows). In the particular one picked as a central test case, turbulent flow down a rearward facing step, variations in numerical predictions were attributed as much to numerical aberrations as to differences in turbulence models used. Indeed, one exercise consisted of asking the computors to use an identical, specified model (the ubiquitous 'k–ε' model) to compute this flow. The resulting predictions varied significantly, even in cases where predictors had used very similar grids.

* Present address: Shell International Petroleum Maatschappy, EP 22.1, P.O. Box 162, 2501 AN, The Hague, Holland

0271–2091/87/080793–31$15.10

Received 16 August 1986
Revised 19 November 1986

At least some of these differences were attributable to fundamental differences in numerical techniques, particularly in the finite-difference formulations used. (No-one attempted a finite-element computation for this flow.) Similar differences were also noted even in predictions of ostensibly less complex flows which could be conveniently attacked using either parabolic (marching) or elliptic (iterative) techniques. It was evident then (1980/81) that numerical viscosity effects, 'rediscovered' many times over the past two decades, could be very significant in calculations of engineering flows. Since practically all commercial or even 'research' codes then available for such flows used necessarily non-uniform grids and only zero- or first-order accurate differencing of the convective terms in the governing equations, there was clearly considerable incentive to develop more accurate, but still robust, numerical techniques for such flows.

The deficiencies of the standard, first-order, hybrid differencing schemes commonly embodied by many engineering codes have been increasingly emphasized over the last decade[2] and a number of more accurate formulations have been proposed. One of the first was the so-called 'skew' (or 'vector') scheme discussed by Raithby and Torrance[3] and Raithby.[4] This was developed to reduce the numerical errors which can arise if significant gradients of the dependent variable exist normal to the streamlines and the flow is oblique to the mesh. It has been extended and applied to a number of complex flow problems by, for example, Lillington[5] and Castro *et al.*[6] Alternative 'higher-order' schemes have been suggested by Leonard,[7] Hodge *et al.*[8] Thompson and Wilkes[9] and Leschziner[10] among others. Rather than taking explicit account of the flow direction as the vector schemes do, the techniques suggested by these authors all use additional nodal points on the grid lines through the central point but outside the basic five point star employed by standard hybrid schemes.

The general character of the various finite difference methods can be deduced from studies of simple model equations which mimic the Navier–Stokes equations; recent examples of this approach can be found in References 11 and 12, but it is not generally possible to *quantify* the numerical errors which will arise in full predictions of the equations. This fact has led to a number of recent exercises in which workers have been invited to use their particular techniques to solve a prescribed flow problem. Unfortunately the results of such comparisons are often rather inconclusive and the difficulties surrounding such exercises are now well recognized. Ideally, of course, one would like to be able to compare numerical predictions of complex flows with exact solutions but there are, as is well known, very few exact solutions of the Navier–Stokes equations for flows containing regions of recirculation. We do not, incidentally, hold the view that laminar flow predictions are useless for assessing likely numerical errors in high Reynolds number turbulent flows. If the particular flow and Reynolds number are chosen sufficiently carefully, we believe that errors in momentum equation solutions can be directly comparable to those that occur in more practical cases. This can be illustrated by reference to the flow studied by Castro *et al.*,[6] a laminar flow around a normal flat plate with a long central downstream splitter plate. At Reynolds numbers around 100, the separated flow region is of a very similar size to that which occurs in the corresponding high Reynolds number (e.g. 10^5) turbulent flow. The irrotational flow surrounding the 'plate + separated wake' must therefore be closely similar in the two cases, so that numerical errors in solution of the momentum equations will be similar. Even within the wake, the 'average' eddy viscosity in the turbulent case must be of the same order as the laminar viscosity in the low Reynolds number case (for $Re \simeq 100$) so that, again, numerical errors will be similar in an overall sense. This flow typifies many real flows of engineering interest which are computationally difficult from a numerical point of view. It contains regions in which convective terms balance 'source' terms (i.e. convection vs. pressure gradients in the momentum equations) and regions in which convection is balanced largely by diffusion (i.e. the turbulent Reynolds stress terms, which are often diffusive-like). Maintaining numerical accuracy

and stability in both flow regimes simultaneously is one of the basic difficulties in computational approaches to complex flows of this sort.

Although there are no non-trivial recirculating flows for which exact analytic solutions are available, there has been considerable progress in developing asymptotically correct solutions for some kinds of bluff-body flows. Theories are usually based on the work of Stewartson (e.g. Reference 13); external flows like the laminar flow over a circular cylinder or flat plate have been studied by Smith,[14,15] who has also obtained solutions for the (upstream) flow over constrictions in pipes and channels.[16] In view of the difficulties in prescribing appropriate numerical boundary conditions in the far field of free flows (e.g. compare Reference 17 with Reference 18), internal flows are especially attractive as possible test cases against which to study the performance of numerical techniques.

The major objective of the work described in this paper was to assess the advantages and disadvantages of some of the relatively new 'higher-order' finite differencing techniques, by applying them to complex, recirculating flows of the kind described above. We have concentrated on the normal flat plate flow previously studied[6] and the step flow studied by Dennis and Smith.[19] Ordinary hybrid differencing schemes, vector schemes and a higher-order scheme akin to that of Hodge *et al.*[8] have been used, and the numerical errors assessed by comparison with analytic solutions where possible, by high-order calculations of predicted momentum balances[20,21] and by some more straightforward analysis of the finite-difference equations. The analytic comparisons are with detailed solutions of the Stokes' flow problem in regions near sharp corners. Here the flow can be described by a stream-function equation, $\nabla^4\psi = 0$, for which there has been some relevant analysis.[22] An additional benefit of this latter rather novel aspect of the work is the verification that the differenced equations are properly set-up near the corners—vector differencing schemes, in particular, require considerable care in this respect.

It should be emphasized that the intention in this work was not simply to produce predictions for the chosen flows which were as accurate as possible. There is no doubt that more specialized techniques (e.g. grid transformations) 'tuned' by using particular features of the flow geometry, would enable more accurate and more efficient predictions to be made.* However, such an approach would be inevitably much less general. Rather, recognizing that general engineering codes usually embody a single particular finite difference scheme despite a possibly wide range of application, we have concentrated on typical examples of the former, testing them by choosing particular problems which embody the more serious numerical difficulties typical of very many real engineering flows.

Section 2 outlines the finite differencing methods used and includes a relatively straightforward (non-dimensional) analysis of the size of the truncation errors corresponding to each. Attention is concentrated on the effects of non-uniform grid spacing, since in practice it is generally not possible to use uniform meshes in engineering calculations. In Sections 3 and 4 typical results of our computations are presented and discussed, with conclusions summarized in Section 5.

2. THE FINITE DIFFERENCE SCHEMES

2.1. *Preliminaries*

It is common practice to write the (two-dimensional) conservation equations for fluid flow, heat energy, scalar transport etc., in the form

* Since the present work was completed Mei and Plotkin[23] have reported some calculations of just that kind, using the streamline/vorticity formulation. They used an appropriate co-ordinate transformation and predicted the 'Dennis and Smith' flow studied in the present work, with results very similar to those reported here.

$$\frac{\partial \rho u \phi}{\partial x} + \frac{\partial \rho v \phi}{\partial y} = \frac{\partial}{\partial x}\left(\Gamma_x \frac{\partial \phi}{\partial x}\right) + \frac{\partial}{\partial y}\left(\Gamma_y \frac{\partial \phi}{\partial y}\right) + s_\phi, \tag{1}$$

where ϕ is the dependent variable, s_ϕ is a source term and $\Gamma_{x,y}$ are 'diffusivities'. In a laminar flow this represents the momentum equations only, so that ϕ is u or v, $\Gamma_{x,y}$ is the laminar viscosity, ν and s_ϕ is the pressure-gradient term. If the flow is turbulent, momentum equations in the form of (1) imply assumptions about the nature of the turbulence, for the $\Gamma_{x,y}$ are then effectively turbulent eddy viscosities. Although there are many turbulence models which eschew the use of eddy-viscosity (e.g. Bradshaw *et al.*'s[24] alternative leads to equations of hyperbolic type) it remains true that the majority of codes in engineering practice use elliptic formulations like equation (1), and solve each relevent equation using the same numerical technique. The coupled problems of determining the pressure field and maintaining continuity are often dealt with by deriving a pressure perturbation equation, casting it in a form similar to equation (1) and solving it using identical algorithms to those used for the basic equations.

We are not concerned here with the precise details of the algorithms used to solve the finite-differenced forms of the differential equations. Provided that these lead to a converged solution (in some sense), the accuracy will depend solely on the nature of the differencing methods used. Certainly, the adequacy of the solution algorithm will often depend on the latter—some differencing methods will be numerically stable only if solved by a certain type of algorithm. However, we believe that these two aspects of the prediction technique are sufficiently separable to enable sensible study of the one to proceed without too much reference to the other. In the present work, a standard alternate direction implicit (ADI) method has been used in all cases, with the well-known SIMPLE algorithm linking the pressure field and mass continuity.[25]

Equation (1) can be written in finite-difference form by integrating over finite control volumes, like that shown in Figure 1, so that

$$A_p \phi_p = \sum_{\text{all } J} A_J \phi_J + s_{\phi.p}, \tag{2}$$

with the assumption that s_ϕ can be assumed constant over the whole cell. The nodes which contribute to the summation term depend on the particular choice of finite-differencing scheme, as do the values of the multiplying coefficients (A_J, etc.). These contain convective and diffusive flow rates. For standard central or one-sided differencing schemes usually only the four immediately adjacent nodes (labelled E, W, N, S in Figure 1 for obvious reasons) are used, enabling equation (2) to be solved implicitly in the x and y directions in turn using standard tridiagonal algorithms (the ADI scheme referred to above). For higher-order schemes, additional

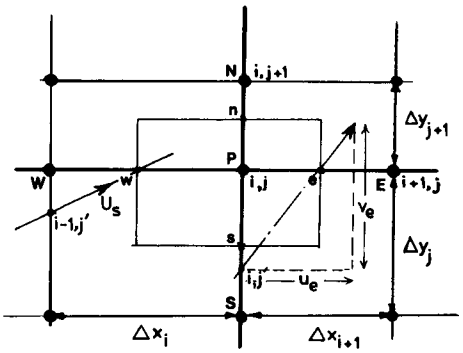

Figure 1. Mesh geometry. Control volume boundaries (containing w, e, n, s) are midway between adjacent boundaries

nodes must be used and, in the present work, to allow use of the same solution algorithms the extra terms arising under the summation in equation (2) are lumped into the source term (s_ϕ) and therefore included explicitly. If the order of the differencing scheme were increased substantially, this would be a very inefficient procedure—the coefficient matrix would be increasingly less sparse—but in the present study it was found to work reasonably well, although convergence rates were undoubtedly rather slower with the higher-order schemes. It is interesting to note in this context that recent work by Marquis[26] has suggested that for higher order differencing schemes using a nine-point star, a pentadiagonal algorithm was no more efficient than the standard tridiagonal algorithm.

All the differencing schemes used the same prescription for the diffusive fluxes in equation (1). Integrating the axial component, for example, over the control volume in Figure 1 gives

$$\iint_{\text{Vol.}} \frac{\partial}{\partial x}\left(\Gamma_x \frac{\partial \phi}{\partial x}\right) \mathrm{d}x\,\mathrm{d}y = \Delta y\left[\left(\Gamma \frac{\partial \phi}{\partial x}\right)_{\mathrm{e}} - \left(\frac{\partial \phi}{\partial x}\right)_{\mathrm{w}}\right],$$

and the usual central difference approximation was used for each derivative, e.g.

$$\left(\Gamma_x \frac{\partial \phi}{\partial x}\right)_{\mathrm{e}} = \Gamma_{\mathrm{e}} \frac{\phi_{i+1} - \phi_i}{\Delta x_{i+1}}.$$

On a uniform mesh system ($\Delta x_i = \Delta x_{i+1}$) the resulting error in ϕ_{xx} is of second order in Δx. In the more common case of an unequal mesh, the error term is of first order in Δx. Note that the diffusive fluxes in this formulation are conservative, in the sense that the flux out of the right hand boundary of the ith cell is identical to that into the left-hand boundary of the $(i+1)$th cell.

In two dimensions, there is an additional error term arising from the unequal mesh spacing in the y-direction. This can be written[27]

$$\tfrac{1}{2}\Delta y_j (r_y - 1) \frac{\partial^2}{\partial x\,\partial y}\left[\Gamma \frac{\partial \phi}{\partial x}\right]_{i,j}.$$

The source term s_ϕ was treated as constant over the control volume. In laminar flows, s_ϕ is generally only the pressure gradient and, as usual, the present scheme employed a staggered mesh so that pressure nodes coincided (on a uniform mesh) with the boundaries of the velocity control volumes. Then

$$s_\phi = \iint_{\text{Vol.}} \frac{\partial p}{\partial x}\,\mathrm{d}x\,\mathrm{d}y \quad \text{(for the axial momentum equation)}$$

and this is put equal to $\Delta y(p_{\mathrm{e}} - p_{\mathrm{w}})$, where p_{e} and p_{w} are known explicitly. On a non-uniform mesh this value is not exactly the same as that at the centre of the velocity control volume, for the pressure nodes do not then coincide exactly with the velocity control volume boundaries. It can be shown that the first order error term consists of a part,

$$\frac{(r_x - 1)}{(r_x + 1)}\left(\Delta x \frac{\partial^2 p}{\partial x^2}\right)_i,$$

arising from the non-uniform x-spacing and a second part,

$$-\frac{1}{4}\frac{r_y - 1}{r_y + 1}\left(\Delta y \frac{\partial^2 p}{\partial x\,\partial y}\right)_j,$$

arising from the non-uniform y-spacing. For a uniform mesh, the error is second order.

For both diffusive and source terms, therefore, the usual schemes are second-order accurate for uniform mesh systems but first-order accurate otherwise, provided that the control volume boundaries are located midway between adjacent nodes. Additional error terms arise if the latter is not true.

It is, of course, the convective terms in equation (1) which generally lead to the most severe accuracy limitations for, as is well known, central difference formulations for these give unphysical oscillations in the solution once the mesh Peclet number ($Pe_i = u_i \Delta x_i / \Gamma$) exceeds two. In the present study, the differences between different schemes lie largely in the methods used to discretize these terms; for completeness these are described separately below, but readers who are familiar with the details could move directly to section 2.5.

2.2. *The standard hybrid scheme (HYDS)*

The well-known hybrid scheme originally suggested by Allen and Southwell[28] uses the (conservative) upwind scheme if the mesh Peclet number exceeds two, with the real diffusive flux contribution being ignored because the resulting error term is at least as large as that,[29] whereas central differencing is used at lower mesh Peclet numbers. This 'smart' upwind scheme has been rediscovered many times and for simple scalar transport in one dimension it gives the correct asymptotic solution at very low and very high Reynolds numbers (Taylor series expansions, indicating the order of the error terms, are not appropriate in the latter case). It does not, however, necessarily lead to correct results at high Reynolds numbers for a non-linear equation (see Reference 30, for example) and it is well known that in the presence either of significant source terms, or of strong cross-flow gradients in two-dimensional cases coupled with mean flow not closely aligned with the grid co-ordinates, the first-order numerical viscosity error terms can be large. It is for these reasons that higher-order schemes for the convective terms have been developed in recent years.

2.3. *The vector (skew) differencing schemes (VDS)*

All vector schemes previously studied are essentially developments of the original proposals of Raithby,[4] who sought a method of reducing the magnitude of the first-order errors which often arise in two-dimensional problems. He suggested a scheme in which, when Re_i exceeds two, the value of ϕ_e, say, is calculated by interpolation between adjacent upstream nodes in a way explicitly dependent on the flow angle. Thus, in Figure 1, if $\tan^{-1}(v_e/u_e) < 2\Delta y_j / \Delta x_{i+1}$, ϕ_e is linearly interpolated between $\phi_{i,j}$ and $\phi_{i,j-1}$.

It can be shown that such a scheme is no more accurate than HDS on the basis of the order of the leading error terms, but the *magnitude* of these terms can be much lower than in standard upwinding because they contain only gradients parallel to the streamline. A principle cause of false diffusion is therefore essentially limited. Note that if $u/v \gg 1$ the scheme reduces to HDS. It should also be emphasized that in an unequal mesh there is a zero-order error term (if the scheme maintains conservation) just as for the HDS. However, tests on model problems have demonstrated the increased accuracy of this scheme,[4,5,21] but since it reduces to the standard HDS when $u/v \gg 1$ there remains the problem of the deleterious effects of significant source terms.

Lillington[5] has suggested a procedure which removes this difficulty by taking account of the source-produced change in ϕ along the streamline. If the interpolated value of ϕ_e is ϕ'_e, say, then the modification amounts to putting

$$\phi_e = \phi'_e + \int_{i,j'}^{e} (S/\rho u_S)\, ds,$$

where u_S is the stream velocity and S is a source correction, taken by using

$$\int_{i,j'}^{e} (S/\rho u_S)\,\mathrm{d}s = sS_{i,j}/(\rho u_S)_e,$$

i.e. by considering S to be a control-volume-averaged property, s is the distance between the i,j' interpolation point and the e point (see Figure 1). It can then be shown that the scheme retains first-order accuracy and remains conservative even on a non-uniform mesh.

In the work presented here, both the standard VDS (described in more detail in References 5 and 6) and this source-corrected version (VDSC) are used. Both can entail the use of nodal values additional to the nearest four used by the HYDS/CDS schemes and neither are invariably diagonally dominant. As mentioned earlier, the additional nodal values are taken from the previous iteration solution and terms including them are lumped explicitly with the source term on the right-hand side of equation (2). This helps to maintain stability; it is rather like a 'deferred corrector' scheme. It can be shown that the source correction amounts in some circumstances to an effective shift of the ϕ nodes by half a cell width. In the case of unidirectional flow, in which convection is balanced largely by a pressure gradient, this therefore leads to an effective shift of the velocity nodes towards the pressure nodes, which is known to be destabilizing. It is consequently not surprising that in some of our calculations at high Reynolds numbers converged solutions could only be obtained if less than the whole of the source correction term were included. Alternative algorithms to the standard ADI method used may have reduced this difficulty somewhat.

Finally, it is emphasized that although the size of the error terms can be substantially reduced with VDSC, it remains formally only a first-order scheme, compared with the second-order nature (on a uniform mesh) of the diffusion and source term differencing techniques. This is perhaps a major reason for the development of alternative 'higher-order' schemes, outlined below.

2.4. *Higher-order differencing schemes (HODS)*

One of the first formally higher-order schemes to be suggested is due to Leonard.[7] This uses two additional nodes one of which is downstream, to difference the convective term by

$$u\frac{\partial\phi}{\partial x} = \frac{u}{6\Delta x_i}(2\phi_{i+1} + 3\phi_i - 6\phi_{i-1} + \phi_{i-2}) \quad (u > 1), \tag{3}$$

or an equivalent expression if $u < 0$. On a uniform grid this is third-order accurate, but since a downstream value is used (ϕ_{i+1}) the scheme exhibits unphysical spatial oscillations (for $Re > 3$). An alternative form of this QUICK procedure is

$$u\frac{\partial\phi}{\partial x} = \frac{u}{8\Delta x_i}(3\phi_{i+1} + 3\phi_i - 7\phi_{i-1} + \phi_{i-2}) \quad (u > 0). \tag{4}$$

Formally this is only second-order accurate, but the coefficient multiplying the Δx_i^2 error term is very small ($-1/24$). On non-uniform grids both these schemes become only *zero*-order accurate, as shown later.

Hodge *et al.*[8] suggested a three-point scheme which is second-order on a uniform grid:

$$u\frac{\partial\phi}{\partial x} = \frac{u}{\Delta x_i}(\tfrac{3}{2}\phi_i - 2\phi_{i-1} + \tfrac{1}{2}\phi_{i-2}) \quad (u > 0),$$

and similarly for $u < 0$. On a non-uniform grid this becomes first-order accurate, so seems more consistent with the usual scheme used for the diffusive terms. Like VDS and QUICK, this scheme is not tridiagonal, but again the convective terms can be appropriately split so that it becomes both

tridiagonal and diagonally dominant, with the additional terms lumped explicitly into the source term. It should be noted that in two dimensions this scheme retains the same order of accuracy, although as usual there are some additional contributions to the error terms if the grid is non-uniform in both directions.

In the present work, numerical computations have been made using this latter scheme (called HODS, for convenience) since it is, formally at least, consistent with the accuracy of the diffusive and source term approximations and is often rather more stable than QUICK.[9]

2.5. *The leading error terms*

It is instructive to compare the error terms which arise in each of the schemes outlined in the previous sections. This can be done by straightforward applications of Taylor's expansion. We concentrate here on the one-dimensional situation, but allow for a non-uniform grid in which the ratio of successive mesh spacings is $\Delta x_{i+1}/\Delta x_i = r$. The control volume boundaries lie midway between adjacent nodes. This minimizes the errors in all cases, with conservation maintained throughout. Note that in two dimensions, if the y-grid is also non-uniform, further error terms sometimes arise, but these are generally of the same *order* as those given below, so do not formally degrade the scheme's accuracy (e.g. see section 2.1).

For the diffusion term, it can be shown that the formulation described in section 2.1 leads to

$$\left(\frac{\partial^2\phi}{\partial x^2}\right)_c = C_0\frac{\partial^2\phi}{\partial x^2} + C_1\Delta x_i\frac{\partial^3\phi}{\partial x^3} + C_2\Delta x_i^2\frac{\partial^4\phi}{\partial x^4} + O(\Delta x_i^3), \tag{5}$$

where the suffix c refers to the calculated value and $C_0 = 1$, $C_1 = 2(r-1)/3(r+1)$ and $C_2 = (1+r^3)/3(1+r)^3$. In the case of the convective term, the calculated first gradient can be written

$$\left(\frac{\partial\phi}{\partial x}\right)_c = C_0\frac{\partial\phi}{\partial x} + C_1\Delta x_i\frac{\partial^2\phi}{\partial x^2} + C_2\Delta x_i^2\frac{\partial^3\phi}{\partial x^3} + O(\Delta x_i^3). \tag{6}$$

In both cases the 'ideal' scheme would have $C_0 = 1$ and $C_1, C_2 = 0$. The actual values of the coefficients C_0, C_1 and C_2 for the convective term are given in Table I, where the two alternative QUICK formulation are labelled '1/6' and '1/8' (see equations (3) and (4)). Figures 2(a)–(c) show the variations of these coefficients as r varies between 0·5 and 1·5 and Figure 3 shows the

Table I. Coefficients of error terms in finite difference representation of the first derivative. Values for uniform grid ($r = \Delta x_{i+1}/\Delta x_i = 1$) are shown in brackets

Scheme	C_0	C_1	C_2
UPW	$\frac{2}{(1+r)}$ (1)	$\frac{-2}{(1+r)^2}$ (−1/2)	$\frac{4}{3(1+r)^3}$ (1/6)
CDS	1 (1)	$\frac{r-1}{r+1}$ (0)	$\frac{2(1+r^3)}{3(1+r)^3}$ (1/6)
HODS	1 (1)	$\frac{-(r-1)}{r(r+1)}$ (0)	$\frac{2(r^2-2r-1)}{3r^2(1+r)^2}$ (−1/3)
QUICK (1/6)	$\frac{2r^2+5r-1}{3r(r+1)}$ (1)	$\frac{2r^4-5r^2+2r+1}{3r^2(r+1)^2}$ (0)	$\frac{2(2r^6+5r^3-3r^2-3r-1)}{9r^3(r+1)^3}$ (0)
QUICK (1/8)	$\frac{3r^2+6r-1}{4r(r+1)}$ (1)	$\frac{3r^4-6r^2+2r+1}{4r^2(r+1)^2}$ (0)	$\frac{r^6+4r^3-3r^2-3r-1}{6r^3(1+r)^3}$ (−1/24)

$$\left(\frac{\partial\phi}{\partial x}\right)_{\text{calc}} = C_0\left(\frac{\partial\phi}{\partial x}\right)_i + C_1\Delta x_i\left(\frac{\partial^2\phi}{\partial x^2}\right)_i + C_2\Delta x_i^2\left(\frac{\partial^2\phi}{\partial x^3}\right)_i + \ldots$$

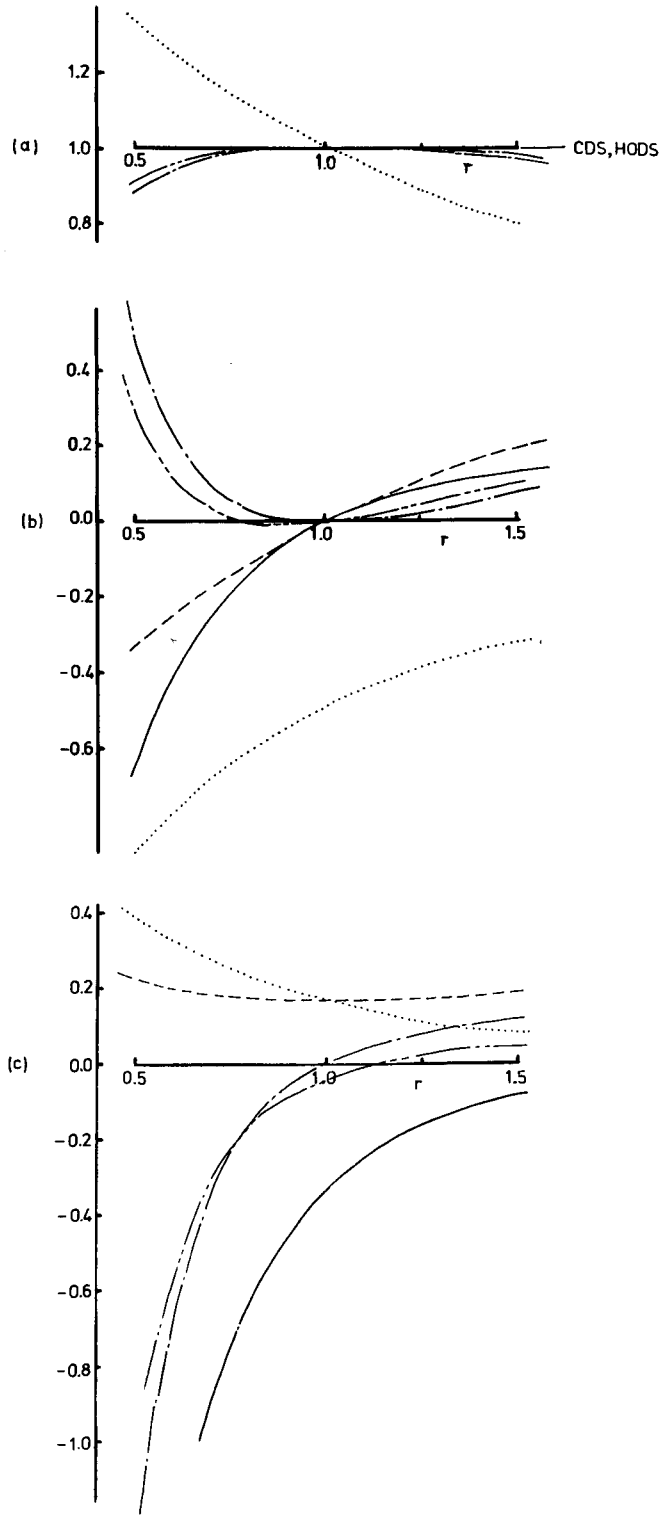

Figure 2. Error term coefficients for the convective term: ....., upwind (UDS); — — — —, central (CDS); ———, higher order upwind (HODS); ——·—— QUICK (1/6); ——··——, QUICK (1/8). (a) C_0; (b) C_1; (c) C_2. See equation (6)

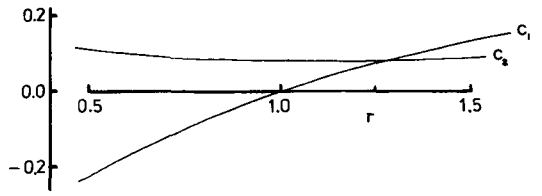

Figure 3. Error term coefficients for the diffusion term (C_0 is unity always); see equation (5)

corresponding results for the diffusive term errors. Note that in one dimension the vector schemes reduce to the standard upwind scheme, so are not included explicitly in the Figures. Note also that these results all assume that $u_e, u_w > 0$; if both are negative the graphs would be inverted about the r-axis, whereas if u_e and u_w had opposite signs additional errors would arise. Indeed normally the formal order of accuracy of the approximations would then be reduced by one.[27]

Now it is recognized that such an analysis has distinct limitations in its usefulness in assessing likely levels of differencing-induced errors in solutions of the (non-linear) Navier–Stokes equations. The actual errors will depend not only on the values of the coefficients but also on the size of the multiplying differentials. However, the results shown in Figure 2 are a clear indication that provided mesh expansion ratios are not too high the Hodge *et al.*[8] HODS scheme is likely to be at least as accurate as central differencing, though not, perhaps, quite as good as the QUICK schemes. The major differences in the coefficients for HODS and QUICK are:

(i) with $u > 0$ and $r < 1$ (or $u < 0$ and $r > 1$) the coefficients of the first-order term (C_1) are of opposite signs (Figure2(b)).
(ii) the coefficients of the second-order term (C_2) have the same trends, but the HODS value is always more negative (Figure 2(c)).

Although it could be argued that in a region where $u > 0$ and $r > 1$ (i.e. the mesh is expanding in the flow direction) HODS errors on the first- and second-order terms are of opposite signs so will tend to cancel—unlike the CDS and QUICK cases—it must be emphasized that this would only occur if the second and third derivatives of ϕ had the *same* sign. Finally, the deficiencies of the standard upwind scheme are obvious from these results. It is worth noting in particular that C_0 differs from unity by less than 10 per cent only if mesh expansion ratios are within the range $0{\cdot}8 < r < 1{\cdot}2$, so that even on grids with quite small expansion ratios there are significant zero-order errors in the convective term approximation.

Much of the above is well known, but its inclusion here serves to emphasized some of the reasons for seeking higher-order differencing schemes.

3. THE FORWARD-FACING STEP FLOW

3.1. Geometry and Gridding

Figure 4 defines the geometry of the first problem to be discussed. A fully developed flow in a two-dimensional channel is distorted by the presence of a severe symmetric constriction in the channel, which provokes upstream separation and, at a sufficiently high Reynolds number, a further separation just downstream of the convex corner. The Reynolds number is defined as $u_m h/v$, where u_m is the mean velocity upstream (2/3 times the peak, centre-line value) and h is the channel half-height. The step height is $h/2$.

As mentioned earlier, an analytic solution for the region $x < 0$ (upstream of the step) has been

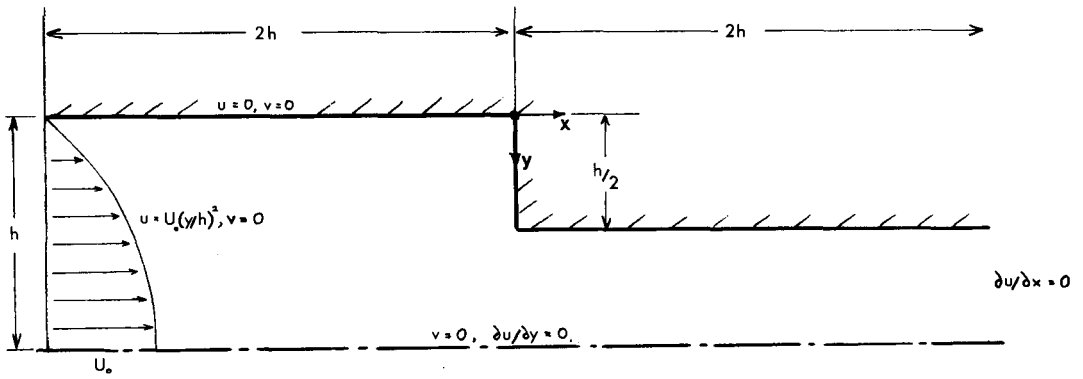

Figure 4. Geometry of forward facing step in a two-dimensional channel. Mean inlet velocity is $2U_0/3$

obtained by Smith;[16] it is asymptotically exact for $Re \gg 1$. Further, Dennis and Smith[19] have undertaken a very careful numerical study of the same flow, using higher-order 'splitting' techniques on the vorticity/stream function equations[31] with a range of uniform grids with mesh spacings down to $h/80$. They used Richardson extrapolation to obtain final numerical solutions, and since at the highest Reynolds numbers these solutions agreed closely with the analytic results it can be safely assumed that their results are accurate throughout the Reynolds number range for $x < 0$. Downstream of the step, however, Dennis and Smith state that their solutions are probably not adequate. We return to this point in due course.

The Dennis and Smith work showed clearly that extending the inlet and/or outlet boundaries beyond $x = 2h$ had no effect on the resulting solutions, so in the current work the solution domain was confined to $-2h < x < 2h$, $0 < y < h$, with $x, y = 0$ at the base of the step. The outlet boundary condition was simply $\partial u/\partial x = 0$ (and hence $v = 0$ from the continuity equation) and on the lower boundary symmetry conditions were imposed—$\partial u/\partial y = 0$, $v = 0$. A specified parabolic velocity profile was used at the inlet, with $u = v = 0$ on all walls. In the case of the HODS scheme, simple first-order upwinding was used at boundaries where appropriate; checks showed that more accurate and complex specifications (requiring more 'image' nodes, for example) had no significant effect on the solutions. Checks were also made to ensure that extensions of the inlet and outlet boundary locations did not affect the results.

During the course of the work various gridding arrangements were used, but attention is concentrated here on the results obtained using essentially two x-grids and three y-grids, the co-ordinates of which are listed in Table II. Note that the coarsest grid, G3, had uniform mesh expansion (or contraction) ratios of about 1·1 in both directions, with $\Delta x, \Delta y = 0{\cdot}012h$ at the corner. The other grids, G1 and G2, which had idential x-nodes but different y-nodes, had somewhat higher (and non-uniform) expansion ratios. At the corner, $\Delta x/h$ was 0·001; $\Delta y/h = 0{\cdot}007$ and 0·003 for G1 and G2, respectively. The mesh spacings were arranged noting that the regions of maximum gradients in the velocities would occur largely near $y = 0, x < 0$ and $y = 0{\cdot}5h, x > 0$. Henceforth all mesh spacings are normalized by h.

Since the plotting of overall streamline patterns is not generally a very sensitive test of the accuracy of numerical solutions of such problems, we prefer to compare the results obtained using the various differencing schemes by looking at some of the quantitative features of the flow. These include, for example, the position of the upstream separation point, the variation of wall vorticity, axial and transverse velocity profiles at various critical positions and pressure distributions. Dennis and Smith[19] presented the first two of these for Reynolds numbers between 10 and 2000, so it is natural to concentrate on those quantities, for they allow us to make a direct comparison

Table II. Nodal values in grids used for the step flow problem. See Figure 1 for co-ordinate definitions

$G1_x$	$G2_x$	$G1_y$	$G2_y$	$G3_x$		$G3_y$
$x<0$	$x>0$	y	y	$x<0$	$x>0$	y
−2·000	0·0005	0·0	0·0	−2·000	0·006	0·000
−1·866	0·0017	0·01	0·0025	−1·905	0·019	0·0135
−1·598	0·0033	0·03	0·0065	−1·714	0·034	0·040
−1·368	0·005	0·055	0·0125	−1·542	0·049	0·0685
−1·170	0·0075	0·08	0·0235	−1·385	0·066	0·0995
−0·999	0·010	0·11	0·038	−1·244	0·085	0·1335
−0·853	0·014	0·15	0·0565	−1·115	0·106	0·1715
−0·727	0·018	0·20	0·0815	−0·999	0·128	0·213
−0·618	0·023	0·25	0·1175	−0·894	0·152	0·2505
−0·525	0·030	0·30	0·168	−0·798	0·179	0·2845
−0·445	0·038	0·35	0·2385	−0·712	0·208	0·3155
−0·376	0·048	0·39	0·311	−0·633	0·240	0·3435
−0·316	0·060	0·425	0·363	−0·562	0·275	0·3685
−0·265	0·075	0·45	0·400	−0·498	0·313	0·392
−0·221	0·094	0·465	0·427	−0·440	0·355	0·4135
−0·183	0·117	0·48	0·446	−0·387	0·401	0·433
−0·151	0·145	0·49	0·4605	−0·339	0·451	0·4505
−0·123	0·180	0·4965	0·4715	−0·296	0·505	0·4665
−0·099	0·222	0·5035	0·480	−0·257	0·565	0·4810
−0·078	0·275	0·51	0·4865	−0·221	0·630	0·4940
−0·060	0·340	0·52	0·4915	−0·189	0·701	0·5060
−0·045	0·420	0·535	0·4955	−0·160	0·779	0·5190
−0·032	0·519	0·55	0·4985	−0·133	0·864	0·5335
−0·022	0·641	0·575	0·5015	−0·109	0·957	0·5495
−0·015	0·790	0·61	0·5045	−0·088	1·059	0·567
−0·010	0·975	0·65	0·5085	−0·068	1·170	0·5865
−0·0064	1·202	0·70	0·5135	−0·050	1·291	0·6080
−0·0038	1·482	0·75	0·520	−0·034	1·424	0·6365
−0·0019	1·827	0·80	0·5285	−0·019	1·569	0·6570
−0·0005	2·000	0·86	0·5395	−0·006	2·000	0·6855
		0·925	0·554			0·7165
		0·975	0·573			0·7505
		1·00	0·5975			0·7880
			0·629			0·8295
			0·6705			0·8750
			0·7335			0·9250
			0·805			0·9750
			0·935			1·000
			1·000			

between the present predictions and the 'baseline' solutions which are believed to be accurate (for $x<0$).

3.2. *Solutions for $x<0$. Wall vorticity and separation*

At $Re=100$, all the schemes were found to yield good agreement with the Dennis and Smith results on the finest grids used. Further, the HODS and VDSC scheme results indicated, on the finest grids, a second very small vortex in the (concave) corner ($x=y=0$). This was not obtained by Dennis and Smith, whose finest grid, although it was uniform, had $\Delta x=\Delta y=0{\cdot}0125$. In the present

case the Δx spacing at the step for the finest grid was only 0·001, although there where only 30 x-nodes in the region $-2 < x < 0$. Evidently $Re = 100$ is sufficiently low to ensure that the diffusive error terms arising from a non-uniform grid (principally the C_1 term, see section 2.5 and Figure 2(b)) are small compared with real diffusion. As is demonstrated below, this is clearly not the case at significantly higher Reynolds numbers.

Figures 5(a) and (b) show the wall vorticity variations obtained at $Re = 500$, compared with the Dennis and Smith results. There are very significant differences, with the HODS results lying closest to the latter. A number of points are of interest. First, considering Figure 5(a), which presents results obtained using the same x-grid (G1/2) and two different y-grids, the G2Y results are in all cases noticeably worse than the G1Y results, despite the fact that near $y = 0$ and $y = 0{\cdot}5$ the former had significantly smaller y-mesh spacings. The most dramatic difference occurs in the VDSC case. Now, as pointed out in section 3.1, the refinement in Δy near $y = 0$ and $y = 0{\cdot}5$ was obtained in G2Y by increasing the grid expansion ratios. As shown in Figure 3 this always leads to increases in the magnitude of the coefficient of the 'diffusive' error term (C_1), so at sufficiently high Reynolds numbers it is possible for these error terms to be comparable with the real diffusion—even in the case of the higher order schemes. In addition, at $Re = 500$ there are substantial areas of the flow field in which mesh Peclet numbers based on Δy and the *lateral* component of velocity are higher than two, so that upwinding (whether HYDS or HODS) is used in the v-component momentum equation rather than central differencing. These results suggest that quite small increases in the mesh expansion ratios can have noticeable effects although, again, it should be emphasized that the wall vorticity is a particularly sensitive indicator.

Figure 5(b) shows wall vorticity results obtained using HYDS and HODS on a grid which has much larger mesh spacings near the corner ($\Delta x = 0{\cdot}012$, $\Delta y = 0{\cdot}012$), but about the same number of nodes and consequently rather smaller expansion ratios everywhere (less than 1·15). The results are compared with those obtained using G1. It is evident that the HODS solution is relatively insensitive to this change, whereas the HYDS results show noticeable differences.

In Figure 6 the VDSC, HYDS and HODS solutions (on grids G1/2) for the axial velocity components around separation are compared. As anticipated from the results in Figure 5(a), there is a marked difference between the two VDSC solutions. The one obtained using G2Y contains large scale 'oscillations' in the u-profile which are markedly reduced in the G1Y solution. Now recall that the G2 grid has a finer distribution of y-nodes around $y = 0{\cdot}5$, but the same x-mesh. This leads to many more mesh cells having a high aspect ratio ($\Delta x/\Delta y$) in regions of the flow where v/u is not negligible, so that the full, vector scheme uses *downstream* nodes in a larger region of the flow. As noted in section 2.3, this has a destabilizing effect, and evidently the Reynolds numbers are sufficiently high in this case to cause unphysical spatial oscillations. Figure 6 includes the results obtained by using the original procedure suggested by Raithby[4] when $\tan^{-1}(v_e/u_e) > 2\Delta y_j/\Delta x_{i+1}$ (see Figure 1). In these circumstances, ϕ_e is set equal to $\phi_{i,j-1}$, rather than interpolating between the latter and $\phi_{i+1,j-1}$. This eliminates the spatial 'wiggles' entirely, although the results are still noticeably different from the more accurate HODS solution (see also Figure 5(a)).

Overall, it seems that the use of HODS has enabled quite an accurate solution to be obtained upstream of the step for $Re = 500$ but, even for this scheme, mesh expansion ratios should be kept low ($r < 1{\cdot}2$, say). The first-order schemes are significantly less accurate and are more sensitive to changes in mesh expansion ratios, as suggested by the analytic results described in section 2.5 (Figure 2). Furthermore, although vector schemes have some apparent advantages, the full version is susceptible to spatial instabilities probably arising from the use of downstream nodal values—this problem is compounded even in regions of relatively low transverse velocities when mesh aspect ratios are high.

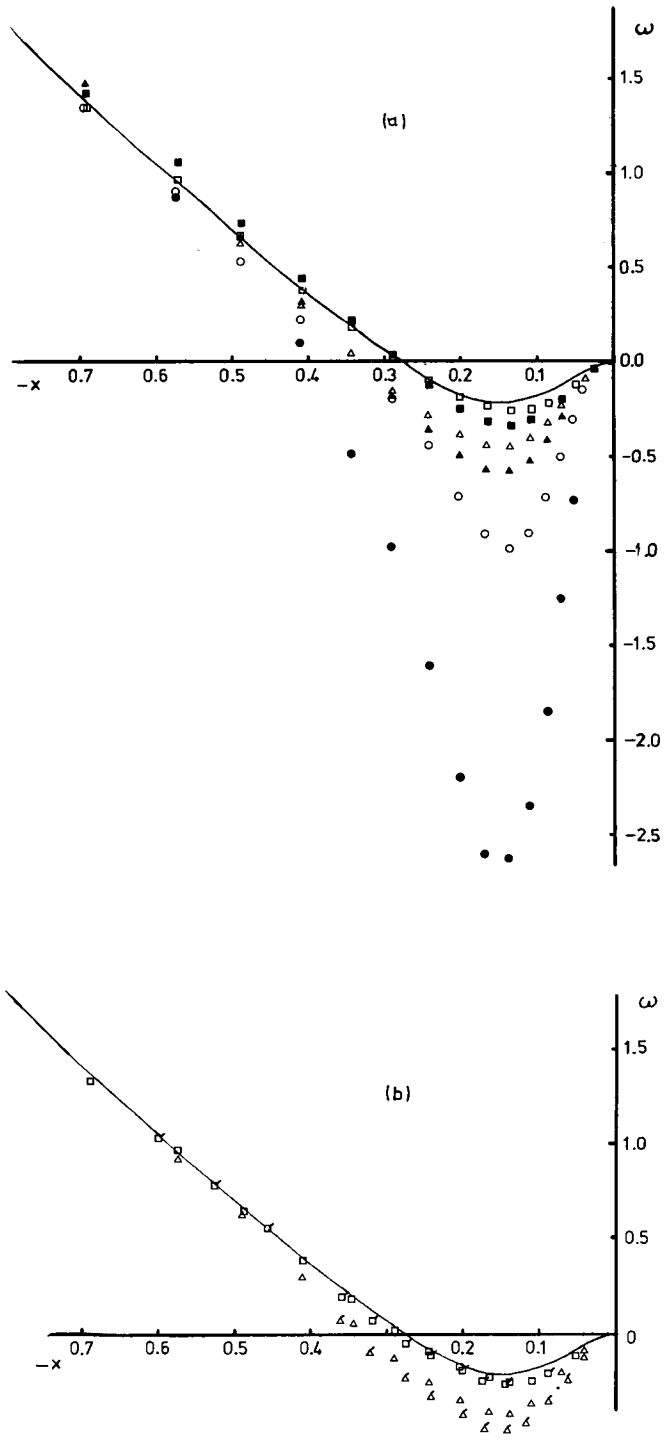

Figure 5. Wall vorticity upstream of step, $Re = 500$. (a) ■, HODS; ▲, HYDS; ●, VDSC: grid 2. Open symbols are for grid G1. ————, Dennis and Smith solution. (b) Legend as in (a) with dashed symbols refering to grid G3 ($\Delta x, \Delta y = 0{\cdot}012$ at the corner)

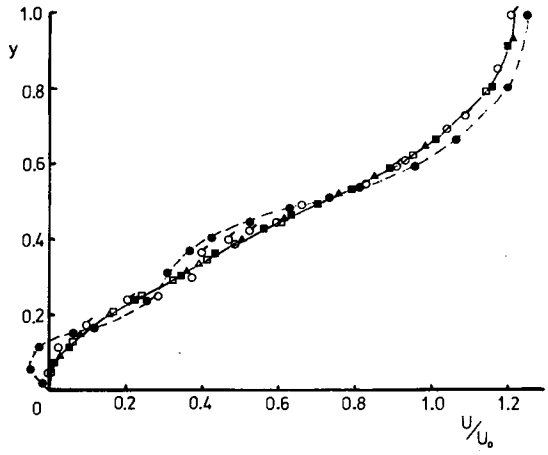

Figure 6. Velocity profiles near separation ($x = -0{\cdot}29$), $Re = 500$. Legend as in Figure 5(a), with ○, VDS (Raithby) on grid G2

3.3. *Solutions for* $x > 0$

3.3.1. $Re = 100$. In the light of the results for $x > 0$ and the statements of Dennis and Smith concerning their $Re = 100$ solutions, little difficulty was anticipated in obtaining reasonably accurate results for this case, at least if HODS were used. In terms of overall flow parameters this turned out to be the case in the sense that wall pressure and velocity profiles obtained from HYDS and HODS solutions on various grids showed close agreement, to graphical accuracy at least, in all cases.

However, in the viscosity-dominated region near the corner this was not the case. In Figure 7 the wall vorticity results are compared with those of Dennis and Smith on their two finest uniform grids ($\Delta x, y = 0{\cdot}0125$ and $0{\cdot}0167$). There are clearly major differences for $x < 0{\cdot}2$. Now the finest grid (in the corner region) used in the present calculations was G2, with $\Delta x = 0{\cdot}001, \Delta y = 0{\cdot}003$ around $x = 0, y = 0.5$ and this is very much finer than the finest grid of Dennis and Smith. Since the vorticity is singular at the corner it seems reasonable that, provided mesh expansion ratio errors are not too important, the G2 solution will be the most accurate near the corner. It should be emphasized that all our computations employed central differencing in this region since the mesh Reynolds numbers are inevitably very low. Defining the Stokes radius as ν/u_m, the G2 grid has about six nodal points (in the x-direction) nearer to the corner than this value—$0{\cdot}0133$ for $Re = 100$—so it was possible to test the internal consistency of the numerical solutions by comparing them with the analytic solution for the viscous flow around the corner. The latter can be obtained by solving the 'slow-flow' approximation to the Navier–Stokes equations for flow in the vicinity of a singular point on a solid boundary.[22,32,33] It will always be valid in a region sufficiently near the singularity, typically within a distance of the order of the Stokes radius from the corner.

3.3.2. The Stokes corner flow. Sufficiently near the corner diffusion dominates and the flow must satisfy the bi-harmonic stream-function equation $\nabla^4\psi = 0$. Blowers[34] has shown, using Weinbaum's[33] solution, that for flow round an external corner of angle $\alpha = 3\pi/4$ the solution is

$$\psi^{(0)} = Ar^m f_1(\theta) + Br^n f_2(\theta),$$

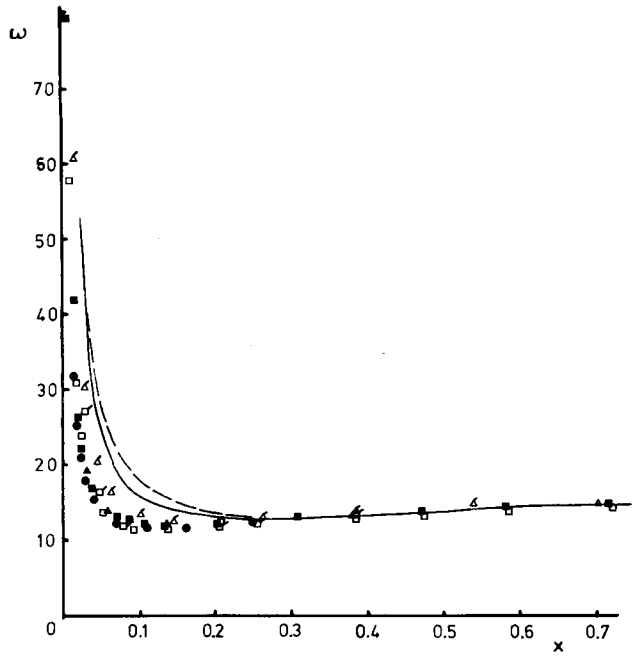

Figure 7. Wall vorticity, $x > 0$, $Re = 100$. ■, HODS; ▲, HYDS; ●, VDSC: grid G2. Open symbols are for grid G1 and dashed symbols are for grid G3. ————, Dennis and Smith (Δx, $\Delta y = h/80$); — — — —, $h/60$

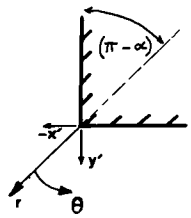

Figure 8. Notation for the viscous corner flow

where

$$f_1(\theta) = \cos(m\theta) + p\cos[(m-2)\theta],$$

and

$$f_2(\theta) = \sin(n\theta) + q\sin[(n-2)\theta]$$

and $m = 1{\cdot}5445$, $n = 1{\cdot}9085$, $p = \cot(m\alpha)$ and $q = -\tan(n\alpha)$. A and B are arbitrary constants corresponding to the symmetric and antisymmetric parts of the solution, whose values depend on the external (inertial) flow field. The polar co-ordinate notation is defined in Figure 8. Higher-order solutions can be obtained from the full Navier–Stokes equations by adding appropriately derived terms to the first-order $\psi^{(0)}$ solution, and it is straightforward to obtain the vorticity distribution from $-\rho\omega = \nabla^2\psi$. The first-order solution is

$$\omega^{(0)} = -\nu[Ar^{m-2}g_1(\theta) + Br^{n-2}g_2(\theta)],$$

with

$$g_1(\theta) = 4p(m-1)\cos[(m-2)\theta]$$

and

$$g_2(\theta) = 4q(n-1)\sin[(n-2)\theta].$$

Now our numerical solutions were obtained from the primitive equations, so it is convenient to use the results for the velocities u and v. These can be easily derived from the ψ solution.

Using the finest corner grid (G2) HODS solution, the two parameters A and B were found by fitting the resulting expression for u to the computed values at two mesh points nearest the corner. Analytic profiles of u and v were then compared with the computed results at all other points around the corner. Table III presents a direct quantitative comparison for the u velocity, for the two cases obtained by forcing agreement at the points ($-0{\cdot}0012$, $-0{\cdot}0015$) and ($-0{\cdot}0012, 0{\cdot}0015$) or ($-0{\cdot}0012$, $0{\cdot}0015$) and (0, $0{\cdot}0015$). The A and B values were $-31{\cdot}1$, $50{\cdot}7$ and $-32{\cdot}0$, $66{\cdot}5$, respectively. Qualitatively it is clear that the agreement is good in the region $x', y' < |0{\cdot}005|$ but becomes less satisfactory at larger distances from the corner. Figure 9 compares the analytic velocity profiles along the lines $x' = 0$, $y' = 0$ with numerical solutions obtained on grids G2 and G3 (the coarsest near the corner) using HYDS, HODS and VDSC. It is evident that not only are the finest grid solutions consistent with the analytic Stokes flow solution near the corner, and accurately so up to a distance equal to about half the Stokes radius ($v/u_m = 0{\cdot}0133$), but also

Table III. Comparison of analytic and numerical solution for u in the corner region. See Figure 8 for x, y definitions

$-x'$	y'	HODS (G2)	$A = -31{\cdot}1$ $B = 50{\cdot}7$ Analytic	$A = -32$ $B = 66{\cdot}5$ Analytic
0·0051	−0·0045	0·866	0·974	0·995
	−0·0015	1·750	1·999	2·024
	+0·0015	3·53	3·75	3·75
	+0·0045	4·97	5·37	5·30
0·00285	−0·0045	0·322	0·355	0·365
	−0·0015	0·955	1·099	1·120
	+0·0015	3·29	3·32	3·33
	0·0045	4·79	5·08	4·99
0·0012	−0·0045	0·057	0·061	0·063
	−0·0015	*0·302*	*0·302*	0·310
	+0·0015	*3·01*	*3·01*	*3·01*
	+0·0045	4·51	4·71	4·60
0·0	0·0015	*2·52*	2·54	*2·52*
	0·0045	4·17	4·31	4·18
	0·0085	5·68	5·90	5·45
−0·001125	0·0015	1·83	1·77	1·72
	0·0045	3·78	3·84	3·67
	0·0085	5·42	5·39	5·07
−0·0025	0·0015	1·29	1·15	1·07
	0·0045	3·29	3·23	3·03
	0·0085	5·06	4·93	4·58
−0·004175	0·0015	0·907	0·794	0·702
	0·0045	2·75	2·585	2·36
	0·0085	4·62	3·362	3·98

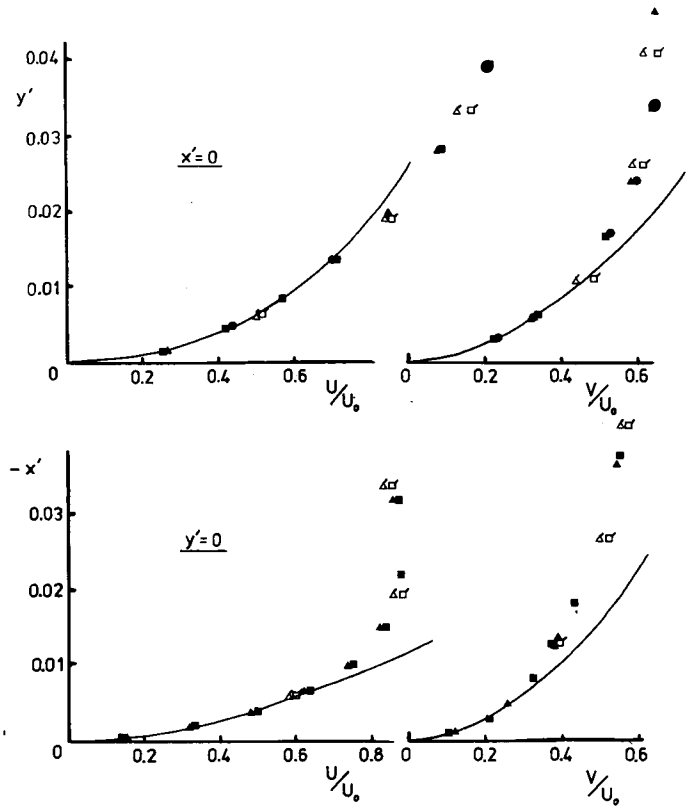

Figure 9. Velocity profiles in the corner region, $Re = 100$. ————, analytic solution with $A = -31{\cdot}1$, $B = 50{\cdot}7$. (The Stokes radius is about 0·013). Legend as in Figure 5(a)

that there are only small differences between the finest and coarsest grid solutions, independent of the differencing scheme used. In this region, of course, central differencing is involved in all the schemes, because of the low mesh Reynolds numbers, but the A and B values are essentially set by the outer inertial flow, so we must again conclude that for the step flow at $Re = 100$, standard hybrid differencing is adequate for overall flow prediction.

It is instructive to compare the wall vorticity predictions with the analytic solution obtained using the fitted A, B values and with the Dennis and Smith predictions. This is done in Figure 10, where only the near corner region is shown; the best fit is obtained using the A, B values found by considering the two nodes just upstream of the step. The finest grid solutions are not too dissimilar from the analytic solution, although computed vorticity values lie consistently higher than those obtained from the latter. As the grid becomes more coarse, the difference increases. Figure 7 shows that the vorticity predictions of Dennis and Smith are considerably higher than our results for $x < 0{\cdot}2$. This is even true for the grid G3 results, which has near-corner mesh sizes not much smaller than those of the finest Dennis and Smith grid. Now the results of Dennis and Smith were obtained by solving the streamline/vorticity equations and this required a somewhat arbitrary procedure to specify boundary conditions near the corner in order to avoid having to use the nodal point coincident with the corner itself, where the vorticity is singular. Blowers[31] has demonstrated the extreme sensitivity of vorticity solutions near the corner to the particular procedure chosen, and it seems that the methods used by Dennis and Smith lead to errors in wall vorticity values for $x > 0$ which are of the same sign as those produced by too coarse a grid. There seems no doubt that the claim of Dennis and Smith that 'graphical accuracy, at the very least, is assured by the finest grid solutions' (Δx, $\Delta y = 0{\cdot}0167$) is somewhat optimistic.

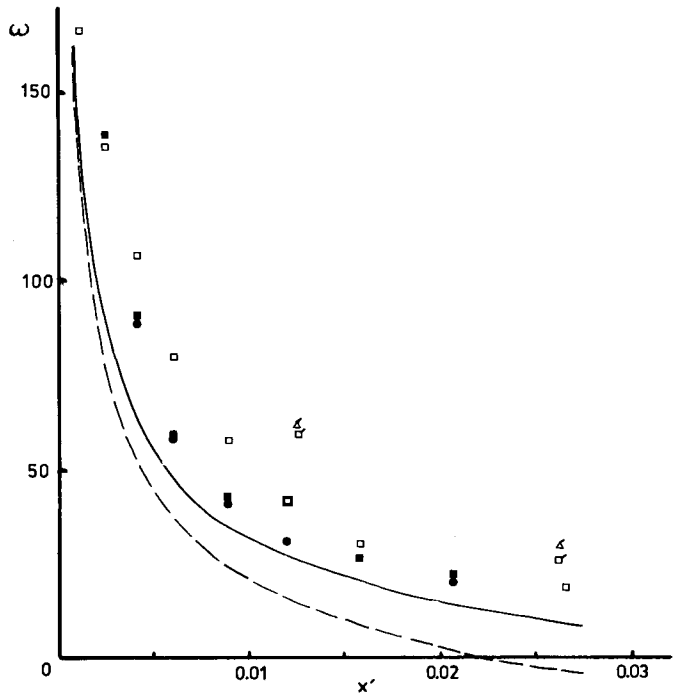

Figure 10. Wall vorticity in the corner region, $Re = 100$. Analytic solution with $A = -31{\cdot}1$, $B = 50{\cdot}7$: ————; $A = -32$, $B = 66{\cdot}5$: — — — —. Legend as in Figure 5(a)

It is worth emphasizing again the relative sensitivity of wall vorticity to numerical deficiencies. Whereas the velocity variations obtained from the HYDS and HODS solutions on grid G3 for $Re = 100$ were virtually indistinguishable for $x < 0$, separation took place noticeably earlier than predicted by the grids having a finer distribution near $x = 0$. As noted earlier, the HODS solutions were less sensitive than the HYDS solutions to grid variations. Similarly, despite quite significant differences in wall vorticity for $x > 0$ (Figure 10) velocity profiles in this region were, again, found to be graphically indistinguishable in all our $Re = 100$ solutions.

We conclude that the overall flow properties can be adequately predicted with hybrid differencing at $Re = 100$, but fine details, such as the exact separation location or wall vorticity near the corner, are rather sensitive to variations in gridding, although less so if higher-order differencing is used.

3.3.3. $Re = 500$. Numerical predictions of wall vorticity obtained for $Re = 500$ are shown in Figure 11. Because of the difficulties with the VDSC solutions discussed in section 3.2, only HYDS and HODS results are shown. It is immediately apparent that in all cases a separated region is predicted, in complete contrast to the finest prediction of Dennis and Smith (with $\Delta x, \Delta y = 0{\cdot}0125$). Even the HYDS solution on the G3 grid, which has mesh spacings similar to those of Dennis and Smith the corner, indicates separation around $x \simeq 0{\cdot}045$ with subsequent reattachment near $x = 0{\cdot}2$. This, again, must indicate the inadequacy of the Dennis and Smith procedure for assigning wall vorticity boundary conditions near $x = 0$. In fact Dennis and Smith explicitly state in this case that 'it is possible that the solution is affected by the presence of the singularity in vorticity at the corner'.

Although the HYDS and HODS solutions on the finest grid (G2) are very close for $x < 0{\cdot}1$, there is substantial divergence further downstream, with the HYDS solution leading to reattachment

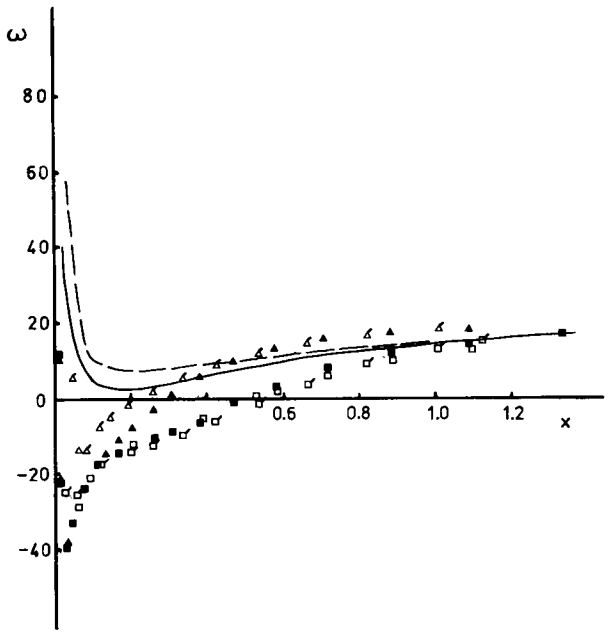

Figure 11. Wall vorticity, $x > 0$, $Re = 500$. Legend as in Figure 7

much earlier than the point suggested by the HODS solution. Beyond separation near $x = 0{\cdot}005$ the larger numerical errors present in the HYDS solutions lead to very significant 'thickening' and subsequent early reattachment of the separated shear layer. This inevitably leads to noticeably different velocity profiles downstream. Figure 12(a), for example, compares profiles at $x = 0$, 0·25 and 1·0. Despite the broad agreement between HYDS and HODS (on the finest grid) at $x = 0$, there is substantial disagreement at $x = 0{\cdot}25$. The larger scale plot in Figure 12(b) emphasizes the increasing differences between HYDS and HODS solutions with distance downstream. Beyond reattachment the differences reduce; this is to be expected since the flow will be asymptotic to the basic Poisseuille channel flow, for which hybrid differencing will be essentially as accurate as higher-order schemes, since longitudinal velocity gradients are identically zero.

For this higher Reynolds number case the region near the corner within which the analytic Stokes' flow solution can be expected to be valid is obviously much more restricted than at $Re = 100$. The Stokes radius is about 0·003 and grid G2 has a few points within that distance from the corner. A fit to the computed u-velocity at the points $(-0{\cdot}0012, 0{\cdot}0015)$ and $(0, 0{\cdot}0015)$ yields $A = -54{\cdot}8$ and $B = 224{\cdot}8$. The ratio $-B/A$ is therefore 4·1, which is about twice its value in the $Re = 100$ case. Recall that since B represents the antisymmetric part of the viscous solution, $-B/A$ is expected to rise as inertial effects in the outer flow become relatively more significant. Figure 13 shows the resulting analytic wall vorticity, compared with the numerical results. All the latter are, again somewhat higher than the former, but the fine grid solutions agree remarkably well with the analytic results if a second-order correction to $\omega^{(0)}$ is included.[34] This leads to a predicted separation point at $x = 0{\cdot}0038$, which is very close to that indicated by the grid G2 results (HODS or HYDS).

Figure 13 also shows the significantly greater sensitivity of HYDS to grid changes; this is evident also in Figure 12(b), from which it is clear that HODS yields a velocity profile near $x = 0$ (with G3) much closer to the fine grid G2 results than the more numerically viscous HYDS can achieve.

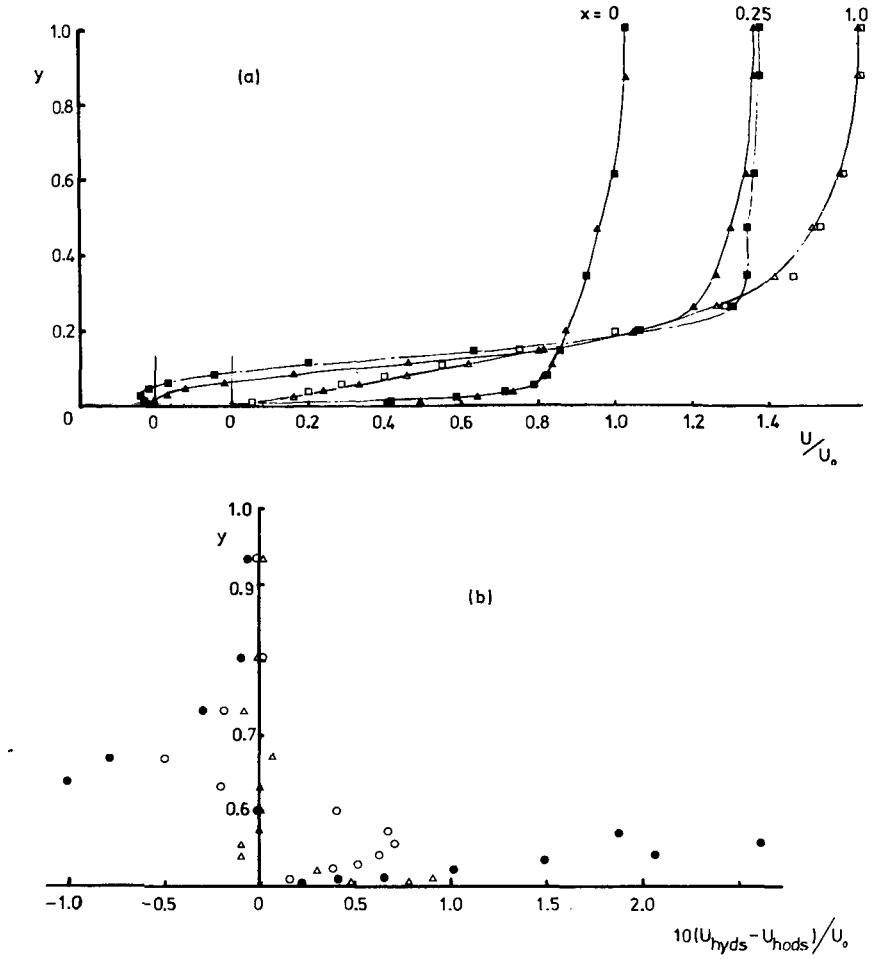

Figure 12. (a) Velocity profiles, $x > 0$, $Re = 500$. ■, HODS; ▲, HYDS; grid G2. Note origin shifts for increasing x (open symbols for $x = 1{\cdot}0$). (b) Difference in velocity profiles for HYDS and HODS, $Re = 500$. $x =$: △, 0·0; ●, 0·25; ○, 1·0

4. THE FLAT PLATE FLOW

4.1. Geometry and Gridding

Figure 14 shows the geometry and boundary conditions for the second problem. This is essentially the same as that previously studied.[6] In the earlier work it was found that generally vector schemes performed much better than the standard hybrid scheme but were inevitably little better than the latter in certain regions of the flow. In particular, along the stagnation streamline total energy was not conserved because there VDS reduces to HYDS. In the present study the work has been extended by adding the source corrections (VDSC) and by using, alternatively, the higher-order upwind scheme (HODS). Because of the interesting possibility of multiple solutions for free wake flows at higher Reynolds numbers (bifurcations) we have concentrated on the case in which the splitter plate is removed and a simple symmetry condition imposed instead. The problem is then a (confined) free wake flow, and a separate study is under way on the asymptotic solution as $Re \to \infty$.[15]

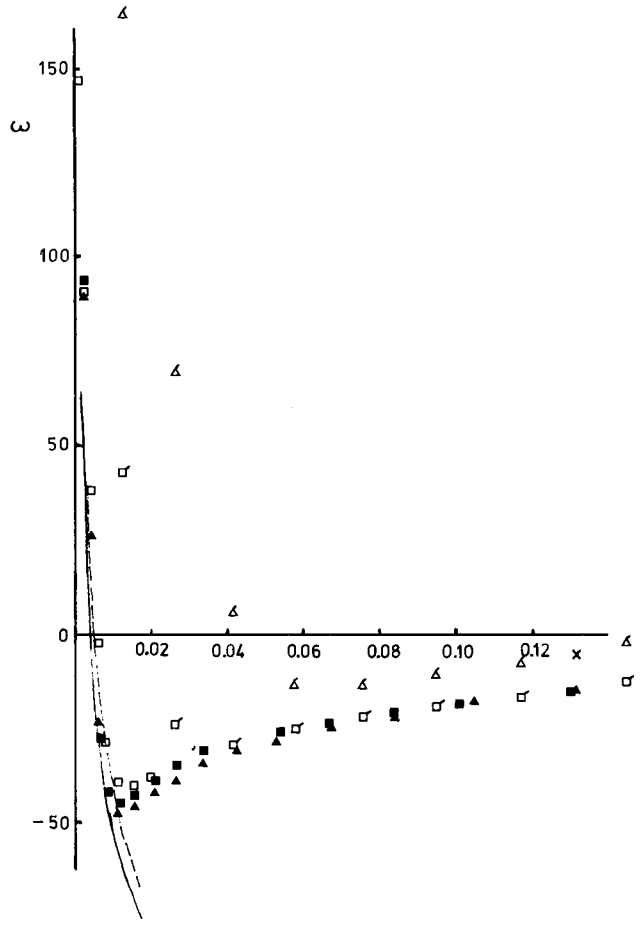

Figure 13. Wall vorticity in the corner region, $x > 0$, $Re = 500$. Legend as in Figure 7. ————, first-order; ———— ————, second-order analytic solution with $A = -54{\cdot}8$, $B = 224{\cdot}8$

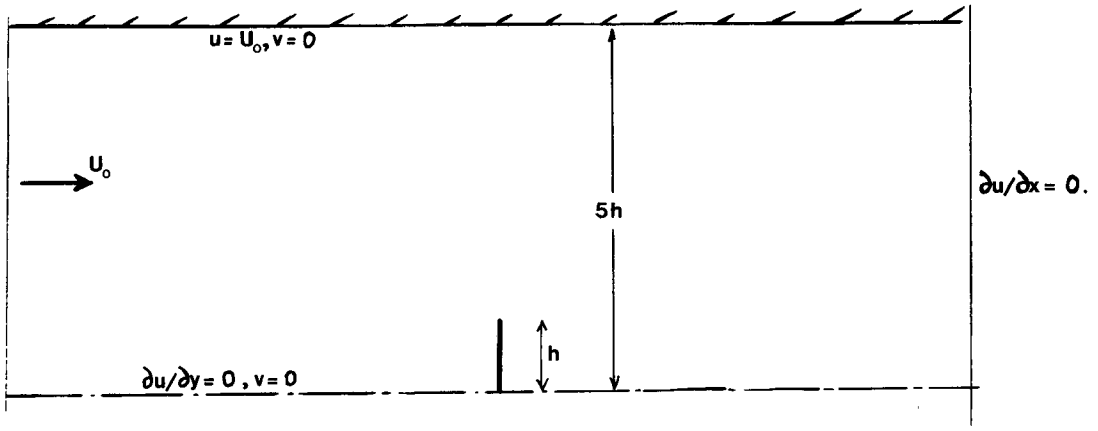

Figure 14. Geometry of flat plate flow. Upstream boundary at $x/h = -20$

The gridding arrangements are also rather different to those used in the earlier work. All the solutions presented here were obtained with the same y-grid, given in Table IV. The x-grid was Reynolds number dependent. Since the Stokes' radius at the corner is inversely proportional to Reynolds number and the boundary layer thickness on the front of the plate is inversely proportional to $\sqrt{Re}$, the upstream grid ($x < 0$) was arranged in two sections. First, the minimum mesh spacing—at the plate itself—was set as α/Re and then there was a uniform expansion *upstream* up to the nominal edge of the boundary layer, taken as $2\beta/\sqrt{Re}$, with usually four to eight

Table IV. Nodal values for basic grid used in $Re = 100$ solutions of the flat plate flow; grid F1, $Re = 100$. See Figure 14 for co-ordinate definition

$x<0$	$x>0$	y
−20·000	0·0050	0·00
−18·182	0·0180	0·02
−14·545	0·0351	0·06
−11·636	0·0570	0·11
−9·308	0·0863	0·16
−7·445	0·124	0·22
−5·955	0·174	0·30
−4·763	0·238	0·40
−3·809	0·322	0·50
−3·045	0·432	0·60
−2·435	0·575	0·70
−1·946	0·762	0·78
−1·555	1·006	0·85
−1·242	1·325	0·90
−0·992	1·740	0·93
−0·791	2·283	0·96
−0·631	2·991	0·98
−0·503	3·914	0·993
−0·400	5·120	1·007
−0·318	6·693	1·02
−0·253	8·746	1·04
−0·200	11·426	1·07
−0·158	14·922	1·11
−0·123	19·485	1·15
−0·0935	25·44	1·19
−0·0689	33·21	1·24
−0·0484	43·35	1·32
−0·0313	56·59	1·42
−0·0170	73·86	1·55
−0·0050	82·50	1·70
		1·90
		2·20
		2·60
		3·05
		3·60
		4·05
		4·40
		4·70
		4·90
		5·00

points within this region. Secondly, a further uniform expansion took the grid from this boundary layer edge to the upstream boundary at $x/h = -20$. Generally α and β were unity and there were 30 points for $-20 < x/h < -\alpha/(2\,Re)$. Downstream of the plate the mesh expanded uniformly over generally 30 points to a downstream location which was a linear function of Re, and typically two to three recirculation region lengths (L_r) beyond the plate. Arguments presented by Castro *et al.*[6] suggest that $L_r \propto Re$ and our higher order solutions all have that behaviour, as shown later. Table IV gives a typical x-grid for $Re = 100$, where $Re = hu/\nu$. The effects of variations in the grid will be discussed where appropriate. Note that for this confined flow the recirculation region width does not change for $Re > 50$ (hence our fixed y-grid), whereas increases in Re lead to increases in x-grid mesh expansion/contraction ratios. Values of the latter for the case given in Table IV are 0·8 (for $-20 < x/h < -2/\sqrt{Re}$), 0·83 (for $-2/\sqrt{Re}\, x/h < -1/Re$) and 1·3 (for $x/h > 1/Re$).

4.2. *The upstream flow, $x < 0$*

It was shown by Castro *et al.*[6] that neither the hybrid nor the simpler vector schemes conserve total energy in regions where the convective terms are balanced largely by pressure gradients. The present results showed that adding the source correction term almost completely eliminated this kind of error at low Reynolds numbers. However, at $Re = 100$ it proved very difficult to obtain a properly converged solution. Adding just half of the total source correction did give a solution, and in that case the error was reduced by only a factor of about two. As noted earlier the source correction has an inherently destabilizing effect and it would seem that unless more robust algorithms for solving the difference equations are used, not all the potential benefit of the source correction will always be realizable.

In Figure 15(a) a comparison of the variation in total head along the upstream stagnation streamline is shown for $Re = 100$, using HYDS, VDSC and HODS; only half the source correction is applied in VDSC. It is evident that HODS generates the smallest errors, although if all the source correction could be applied in the VDSC case the latter would probably be equally good. The errors in the HODS solution arise from the non-uniform grid; the contraction ratio in the x-grid was 0·8 over most of the $x < 0$ region and this is clearly sufficiently far from unity to lead to

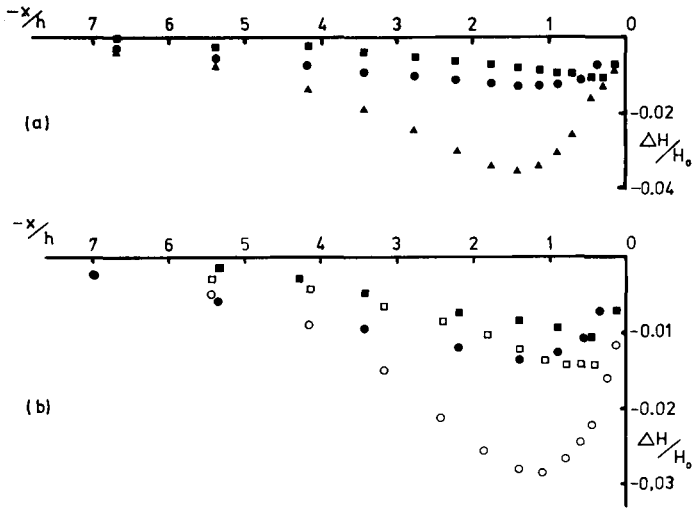

Figure 15. Total head variations along the upstream stagnation streamline at $Re = 100$: (a) ▲, HYDS; ●, VDSC; ■, HODS. Grid F1. (b) ●, VDSC; ■, HODS. Grid F1. Open symbols are for grid F2

perceptible, but small, errors (see Figure 2). Since the inlet velocity was constant across the channel, the total head should have remained at its uniform inlet value everywhere outside the viscous regions—not simply along the stagnation streamline. Further plots of $\Delta H/H_0$ against x/h at various y/h confirmed the above conclusion that HODS was generally significantly better at conserving energy, even in regions of strong lateral velocities and cross-stream gradients, than any of the other schemes (VDS, VDSC or HYDS). In addition, it was consistently easier to obtain converged solutions than it was using the VDSC scheme.

As found in the forward-facing step flow, HODS was also much less sensitive to changes in grid expansion ratios. Figure 15(b) illustrates this. The total head changes for VDSC and HODS at $Re = 100$ shown in Figure 15(a) are compared with those which occur using a rather different x-grid, in which only 24 points were used for $x < 0$ (F2). The grid contraction ratio was consequently rather smaller (0·77, cf. 0·80). It is evident that the difference in ΔH for the two grids is typically three times larger for the VDSC solution than for the HODS solution.

Careful scrutiny of the solutions for $x < 0$ showed in addition that the VDSC results contained 'wiggles' which grew larger with Reynolds number but were entirely absent in the HODS results. It was also found that increases in grid refinement could lead to *larger* instabilities, as found earlier (section 3.2). Tests showed that the 'wiggles' were not in this case the result of the inclusion of the source term in the VDS scheme and neither were they a result of using the *full* vector scheme rather than the original simpler Raithby version. They were symptomatic of the increasing difficulty in obtaining convergence as the Reynolds number was increased.

It is worth pointing out that in this flow, even at $Re = 100$, there were substantial areas of the flow domain in which *lateral* mesh Reynolds numbers ($\Delta yv/\nu$) exceed two. Figure 16 shows part of the boundaries of these regions. This certainly increases the possibilities of spatial instabilities in VDSC solutions and may well be partly the cause of those noted above and also those in the $Re = 500$ step flow solutions (Figure 6).

4.3. *The downstream flow, $x > 0$*

In the earlier study it was found that a Galerkin finite element solution of this flow—but with a downstream splitter plate—gave a rather thicker separated shear layer than the VDS solution at the same x/h, despite a significantly longer distance to reattachment. Figure 17 shows velocity profiles just downstream of separation ($x/h = 0{\cdot}5$) obtained from VDSC and HODS solutions of the $Re = 100$ flow. A similar difference is apparent, with the HODS profile having a rather lower velocity gradient in the shear layer. The VDSC solution looks much less reasonable near the outer edge of the shear layer and it would seem that the possible 'overshoots' inherent in the scheme are

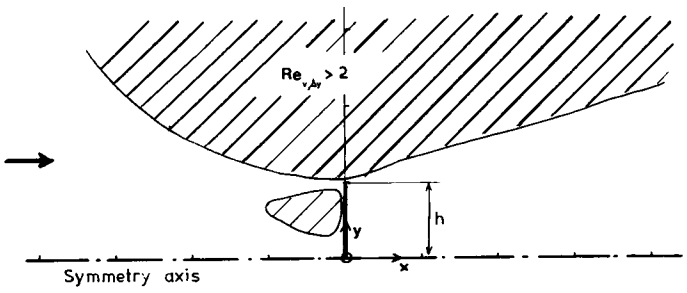

Figure 16. Hatched regions show (part) of the area in which the lateral mesh Reynolds number exceeds two. Longitudinal mesh Reynolds numbers were below two only in an extremely small region around the plate. The Figure is to scale and was obtained from results on grid F1 at $Re = 100$

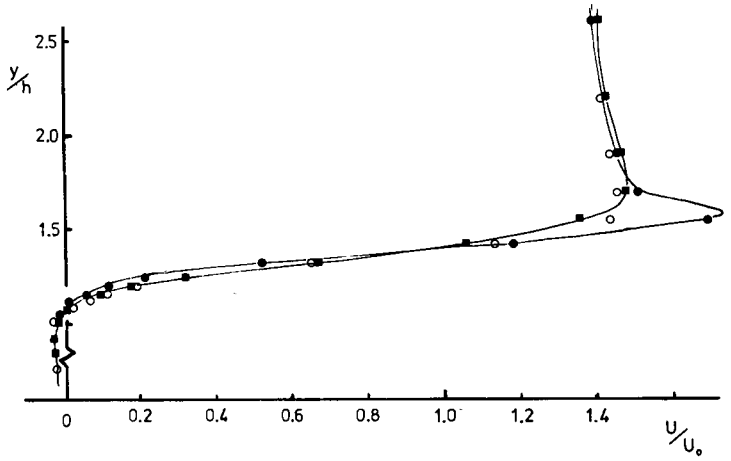

Figure 17. Velocity profiles at $x/h = 0{\cdot}5$, $Re = 100$. ■, HODS; ●, VDSC; ○, VDS (Raithby)

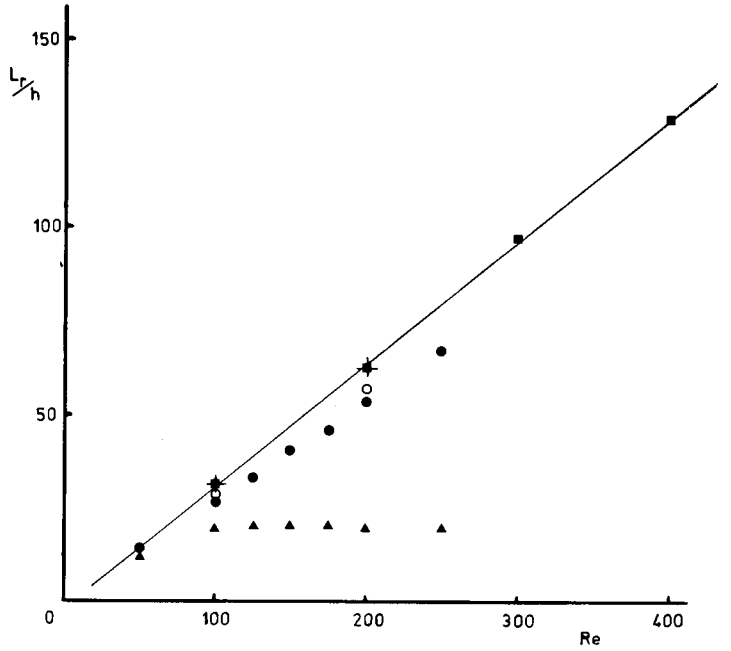

Figure 18. Length of the recirculating wake. ■, HODS; ●, VDSC; ▲, HYDS; ○, VDSC on a 70 × 40 grid; +, finite element results

significant in this region. This could be the cause of the higher velocity gradients, which are maintained throughout the wake flow. Again, the 'wake closure' point nevertheless occurs significantly further downstream in the HODS solution. (Reattachment is an inappropriate term in the present case without a splitter plate.) HODS gives $L_r/h = 31{\cdot}4$, compared with the VDSC result of 26·5. The simple vector scheme (VDS) reduces this overshoot substantially but also gives a low value of $L_r/h(26)$.

Figure 18 shows the variation of L_r/h with Re, obtained using HYDS, VDSC and HODS. Two

additional results from a Galerkin finite element solution are included (Cliffe, private communication) and it is gratifying that the HODS results are very close to these. The standard hybrid scheme is of course quite unsatisfactory; once $Re > 100$, the solutions become independent of Re since the viscosity is virtually all 'numerical'. We were also able to obtain some VDSC solutions on a 70 × 40 grid, which was essentially identical to the basic 60 × 40 grid for $x < 0$ but had 10 extra nodes for $x > 0$ (i.e. 40 instead of 30). In this case converged solutions at $Re = 100$ and 200 could be obtained with 0·7 of the full source correction included. The L_r results are included in Figure 18 and it seems that further refinement could lead to solutions close to HODS and finite element results, at least as far as the L_r value is concerned.

Tests with different grids showed again a much greater dependence of the VDSC solutions on the grid expansion ratios and on details of the grid around the separation point. The centre-line velocity variations for $x > 0$ shown in Figure 19 typify these effects. Figure 19(a) shows results for HODS on the basic grid (F1, Table IV), a grid in which the x-mesh spacing at the fence was five times that in the basic grid (i.e. 0·05) with 24 points in $x < 0$ and 36 for $x > 0$ (F2), and a grid which had the same basic F1 mesh at the plate but only 20 points for $x < 0$ and 40 for $x > 0$ (F3). In addition a further coarser grid solution is shown, with 20 points for $x < 0$, 20 for $x > 0$ and a mesh size at the plate of twice the basic value (F4). This grid has only two x-nodes in the downstream half of the recirculating region! Figure 19(b) shows corresponding results obtained using VDSC. Details of the grid expansion ratios are given in Table V.

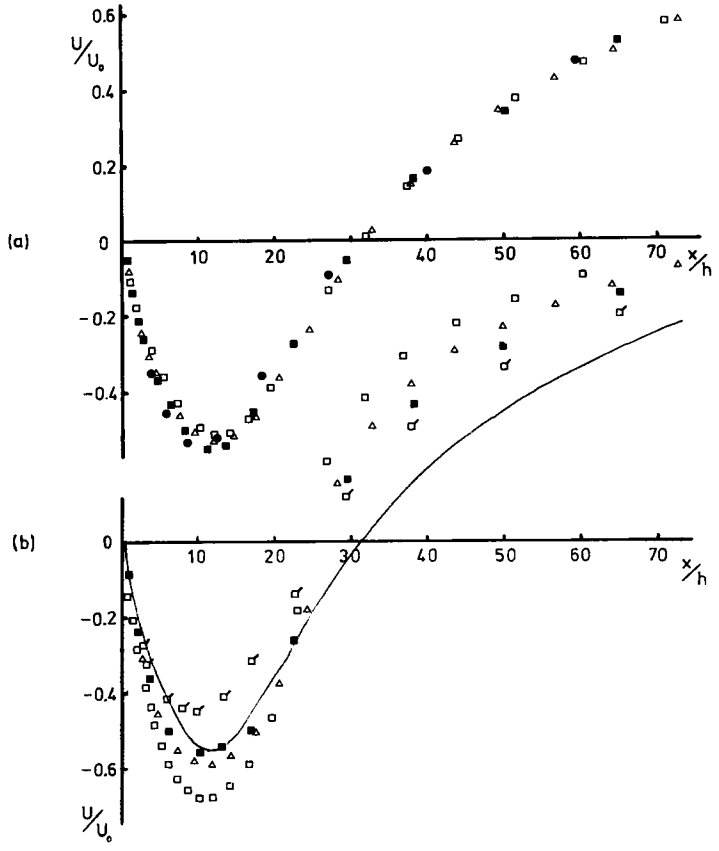

Figure 19. Wake centre-line velocity variations, $Re = 100$. Grid: ■, F1; □, F2; △, F3; ●, F4. (a) HODS. (b) VDSC; ⊡, F1; VDS (Raithby); ————, smooth line through HODS results in (a)

Table V. Salient details for grids used for flat plate solutions

x	y	Δx at fence	No. of nodes $x<0$	r values $x<0$	$x>0$
F1	60 × 40	0·01	30	1·25	1·30
F2	60 × 40	0·05	24	1·21	1·17
F3	60 × 40	0·01	20	1·3	1·12
F4	40 × 40	0·02	20	1·2	1·5

Two major points should be noted. First, it is clear that the VDSC solutions give a much more rapid velocity recovery through the wake closure point than shown by the HODS results. Secondly, whereas the HODS results are practically independent of the grid details—even the course 40 × 40 solution is remarkably close to the others—this is not the case for the VDSC results. These show a continuous trend of *increasing* velocity recovery rate for *decreasing* expansion ratio in the wake region, so this effect must be a result of increasing the mesh spacings around separation (F1–F2) or decreasing the contraction ratios for $x<0$ (F1–F3). The former seems rather more likely and certainly leads to the largest effect.

It should also be noted that even for F1 the mesh spacing at the fence tip ($\Delta x = 0{\cdot}01, \Delta y = 0{\cdot}014$) is of the same order as the Stokes radius ($O(\nu/U_0)$), so we cannot make sensible comparisons between numerical results and the analytic Stokes' flow solution for the corner region. This would require a grid with much smaller mesh spacings near the corner and correspondingly larger grid expansion ratios unless many more grid nodes were used. However, our earlier work showed that it was more important to maintain accuracy in the irrotational region up to and just outside the separating boundary layer than to resolve the boundary layer itself. The present work confirms that, and Figure 20 shows that HODS can be used to obtain solutions up to at least $Re = 500$ which, apart from the appropriate axial scaling with Re for $x>0$, are accurately independent of Re. Details of the viscous regions very near the plate remain Reynolds number dependent, of course, as pressure distributions near the plate tip indicated. We believe that the result $L_r/h = 0{\cdot}325\,Re - 2$ is close to the exact solution for $Re > 100$. In addition, the plate base pressure and drag coefficients, C_{pb} and C_d, were essentially constant at $-1{\cdot}87$ and 2·5, respectively, once the Reynolds number exceeded about 200.

5. CONCLUSIONS

The overall conclusions from these studies can be summarized as follows. First, for the forward-facing step flow, standard hybrid differencing solutions were not significantly less accurate than those obtained using higher-order algorithms or vector schemes, provided the Reynolds number was low (say, less than 100). Solutions obtained on the finest grids were close to those given by Dennis and Smith[19] upstream of the step itself, and increases of mesh size near the corner by even an order of magnitude only marginally effected the solution away from the corner. Around the corner itself, however, the results were noticeably different from those of Dennis and Smith, even on a similar grid. On the finest grid the solutions at $Re = 100$ are consistent with analytic solutions of the Stokes' flow problem, irrespective of the differencing scheme used, since all the latter reduce to central differencing near the corner.

At high Reynolds numbers hybrid or vector differencing became increasingly inadequate, although in all cases and on all grids separation beyond $x = 0$ was predicted, in contrast to the

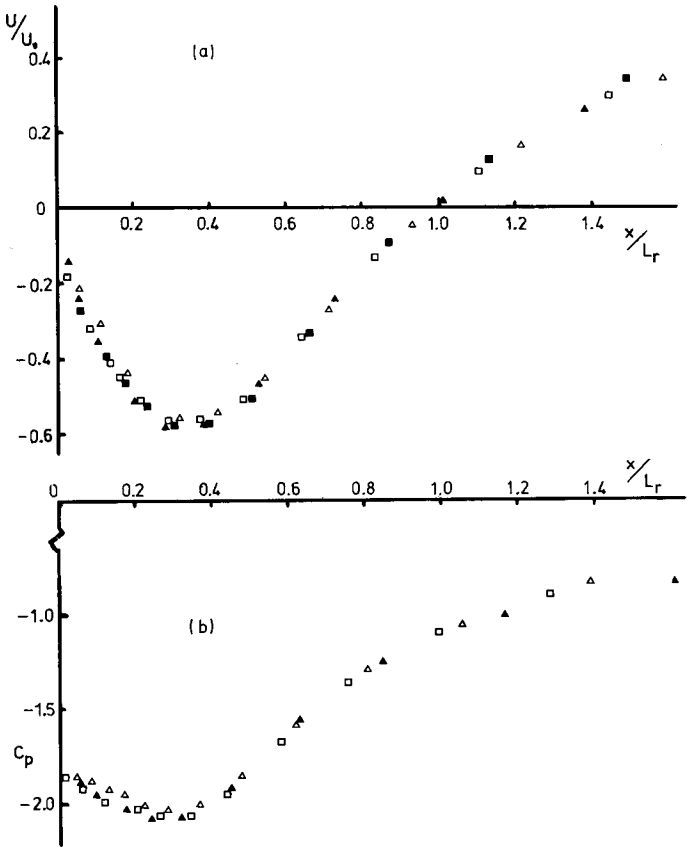

Figure 20. Wake centre-line velocity and static pressure variations, HODS. $Re =$: △,100; □, 200; ■, 400; ▲, 500 ($C_p = (p - p_0)/\frac{1}{2}\rho U_0^2$)

results of Dennis and Smith. For $x < 0$, the higher-order scheme gave a solution very similar to that of Dennis and Smith. For $x > 0$ hybrid differencing caused early reattachment. We believe that the solutions for the forward-facing step flow obtained using HODS are quite accurate (at all Reynolds numbers) throughout the whole flow domain, even in the case of the coarsest grid solution. It does not seem necessary to use extremely fine mesh spacings *everywhere*, so that provided mesh expansion ratios are not too high, accurate solutions can be obtained using grids with *fewer* nodes than in the finest Dennis and Smith[19] solutions.

Secondly, it is emphasized that only the linear higher order upwind scheme remains formally first-order accurate on a non-uniform grid (provided that control volume boundaries are located half way between the grid nodes); QUICK schemes are only zero-order accurate on non-uniform grids. The predictions confirm the implications of the numerical analysis (Figure 2) that non-uniform grids can lead to significant zero-order errors in the simpler schemes. In addition, hybrid and vector schemes show increasing sensitivity to changes in mesh expansion ratio as the Reynolds number rises. This effect was demonstrated by the results for both flows studied. It is much less significant in the case of the higher-order upwind scheme.

Thirdly, vector schemes were found to be susceptible to spatial instabilities and/or overshoots, as previous workers have found. It was shown that in some circumstances high aspect ratio control volumes in the grid can give particular difficulty, but in any case for flow angles other than

0 and 45° to the grid lines the vector schemes are not necessarily diagonally dominant. There is therefore always the possibility of spatial wiggles developing in the solutions, and this tendency will increase with mesh Reynolds number. In contrast to the vector scheme solutions, HODS solutions of the flat plate problem appeared to be quite accurate; they showed the correct trends with Reynolds number and agreed closely with Galerkin finite element solutions.

In the light of the above points, our major conclusion is that the higher-order upwind scheme is by far the best differencing scheme to use for the convective terms in the momentum equations, at least compared with standard hybrid or any of the vector schemes. It is diagonally dominant and therefore stable and is easier to code than either vector schemes or the formally (on a uniform grid) more accurate QUICK methods. The latter can give oscillations and are rather less robust than HODS. We do not believe that our results would be very different if alternative algorithms for solving the differenced equations had been used.

Although we have not as yet studied HODS in the context of turbulent flows, there seems no reason to suppose that this conclusion would change. Indeed, in view of the additional inter-equation coupling and non-linearities it may well turn out that HODS is relatively even better in turbulent flows than in those we have studied. However, careful and detailed investigations of its performance in well-chosen turbulent flows should obviously be carried out.

ACKNOWLEDGEMENTS

This work was supported jointly by the U.K. Science and Engineering Research Council, the U.K. Atomic Energy Authority (Harwell) and Atkins R & D, whose financial support (of JMJ) is gratefully acknowledged.

REFERENCES

1. S. J. Kline, B. J. Cantwell and G. M. Lilley, *The 1980/81 AFOSR-HTTM-STANFORD Conference on Complex Turbulent Flows*, Thermosciences Division, Mech. Eng. Dept., Stanford University, 1982.
2. P. M. Gresho and R. L. Lee, *Computers and Fluids*, **9**, 223 (1981).
3. G. D. Raithby and K. E. Torrance, *Computers and Fluids*, **2**, 191 (1974).
4. G. D. Raithby, *Comp. Meth. Appl. Mech. Eng.*, **9**, 153 (1976).
5. J. N. Lillington, 'A vector upstream differencing scheme for problems in fluid flow involving significant source terms in steady-state linear systems', *Int. j. numer. methods fluids*, **1**, 3–16 (1981).
6. I. P. Castro, K. A. Cliffe and M. J. Norgett, 'Numerical predictions of the laminar flow over a normal flat plate', *Int. j. numer. methods fluids*, **2**, 61–88 (1982).
7. B. P. Leonard, *Comp. Meth. Appl. Mech. Eng.*, **19**, 59 (1979).
8. J. K. Hodge, A. L. Stone and T. E. Miller, *AIAA Journal*, **17**, 458 (1979).
9. C. P. Thompson and N. S. Wilkes, *Harwell Report AERE-R10493*, 1982.
10. M. A. Leschziner, *Comp. Meth. Appl. Mech. Eng.*, **23**, 293 (1980).
11. M. K. Patel and N. C. Markatos, 'An evaluation of eight discretization schemes for two-dimensional convection–diffusion equations', *Int. j. numer. methods fluids*, **6**, 129–154 (1986).
12. W. Shyy, *J. Comp. Phys.*, **57**, 415 (1985).
13. K. Stewartson, *Adv. Appl. Mech.*, **14**, 145 (1974).
14. F. T. Smith, *J. Fluid Mech.*, **92**, 171 (1979).
15. F. T. Smith, *J. Fluid Mech.*, **155**, 175 (1985).
16. F. T. Smith, *J. Fluid Mech.*, **90**, 725 (1979).
17. B. Fornberg, *J. Fluid Mech.*, **98**, 819 (1980).
18. F. T. Smith, *J. Fluid Mech.*, **113**, 407 (1981).
19. S. C. R. Dennis and F. T. Smith, *Proc. Roy. Soc. Lond. A*, **372**, 393 (1980).
20. J. J. McGuirk and W. Rodi, *J. Fluid Mech.*, **86**, 761 (1978).
21. I. P. Castro, in Durst and Launder (eds), *Turbulent shear flows I*, Springer-Verlag, 1979.
22. H. K. Moffat, *J. Fluid Mech.*, **18**, 1 (1974).
23. R. W. Mei and A. Plotkin, *AIAAJ.* **24**, 1106 (1986).
24. P. Bradshaw D. H. Ferris and N. P. Attwell, *J. Fluid Mech.*, **28**, 593 (1967).

25. S. V. Patankar and D. B. Spalding, *Int. J. Heat and Mass Transfer*, **15,** 1787 (1972).
26. A. J. Marquis, *Ph.D. Thesis,* Imperial College, London, 1986.
27. J. N. Lillington, *Winfrith Report AEEW-M1833*, 1980.
28. D. N. Allen and R. V. Southwell, *Quart. J. Mech. App. Math.*, **8,** 129 (1955).
29. P. J. Roache, *Computational Fluid Dynamics*, Hermosa, Albuquerque, 1972.
30. I. P. Castro, in Taylor, Morgan and Brebbia (eds), *Proc. of Numerical Methods in Laminar and Turbulent Flows*, Pentech Press, 1978.
31. S. C. R. Dennis and J. D. Hudson, in Taylor, Morgan and Brebbia (eds), *Proc. of Numerical Methods in Laminar and Turbulent Flows*, Pentech Press, 1978.
32. W. R. Dean and P. E. Montagnon, *Proc. Camp. Phil. Soc.*, **45,** 389 (1949).
33. S. Weinbaum, *J. Fluid Mech.*, **33,** 38 (1968).
34. R. M. Blowers, 'The calculation by finite differences of steady two-dimensional laminar flow in a T-junction', *Ph.D. Thesis*, University of Surrey, 1973.